Int. J. Heat Mass Transfer. Vol. 22, pp. 371–382
© Pergamon Press Ltd. 1979. Printed in Great Britain
0017-9310/79/0301-0371 $02.00/0

SOLUTION OF THE TWO PHASE BOUNDARY-LAYER EQUATIONS FOR LAMINAR FILM CONDENSATION OF VAPOUR FLOWING PERPENDICULAR TO A HORIZONTAL CYLINDER

E. S. GADDIS

Institut für Thermische Verfahrenstechnik, Technische Universität
Clausthal, Leibnizstraße 15, 3392 Clausthal-Zellerfeld, FRG

(*Received* 20 *February* 1978)

Abstract—A method is presented for solving the two phase boundary-layer equations for the condensation of a flowing vapour on a horizontal cylinder. The three governing partial differential equations are transformed into ordinary differential equations, the number of which depends on the accuracy required in the solution. The numerical solutions give the distribution of the local values of the Nusselt number on the periphery of the cylinder as a function of the different governing parameters.

NOMENCLATURE

a, tube radius;
A, function of Y (equation 61);
b, coefficient (equation 33);
c, specific heat;
d, function of Y (equations 54, 56);
D, function of Y (equations 42, 46);
E, function of Y (equation 64);
f, function of Y (equation 50);
F, function of Y (equation 32);
g, acceleration of gravity;
Ga, Galileo number $[=(2a)^3 g/\nu_l^2]$;
h, heat-transfer coefficient;
i, integer;
I, constant (equation 78)
j, integer;
k, thermal conductivity;
L, latent heat of condensation;
m, integer;
n, integer;
N_{lg}, dimensionless number (equation 26);
N_{lp}, dimensionless number (equation 27);
N_{vp}, dimensionless number (equation 51);
Nu, Nusselt number $(=2ah/k_l)$;
p, pressure;
P, function of Y (equation 79);
Ph, phase change number $[=c_l(T_{sat}-T_w)/L]$;
Pr, liquid Prandtl number $(=c_l\mu_l/k_l)$;
q_w, wall heat flux (+ve in −ve y direction);
Q, rate of heat flow per unit tube length between $x=0$ and x;
r, integer;
R_d, density ratio $(=\rho_l/\rho_v)$;
R_ν, kinematic viscosity ratio $(=\nu_l/\nu_v)$;
Re, Reynolds number $(=2aU_\infty/\nu_v)$;
s, distance along the tube circumference;
T, temperature;
ΔT, temperature difference $(=T_{sat}-T_w)$;
u, velocity in the direction of the x axis;
u^*, dimensionless velocity $(=ua/\nu)$;
U_∞, undisturbed vapour velocity;
v, velocity in the direction of the y axis;
w, constant (equation 57);
W, constant (equation 35);
x, distance along the liquid–vapour interface;
y, distance perpendicular to the liquid–vapour interface;
Y, dimensionless distance perpendicular to liquid–vapour interface $(=y/\delta)$.

Greek symbols

α, thermal diffusivity $(=k/\rho c)$;
γ, coefficient (equation 83);
δ, condensate thickness;
Δ, dimensionless condensate thickness $(=\delta/a)$;
ϕ, dimensionless distance along liquid–vapour interface $(=x/a)$;
ρ, density;
ν, kinematic viscosity;
μ, dynamic viscosity;
ψ, stream function;
ψ^*, dimensionless stream function $(=\psi/\nu)$;
θ, dimensionless temperature (equation 59);
ε, constant (equation 36).

Subscripts

l, for liquid;
v, for vapour;

0, at $\phi = 0$;
m, mean value;
w, at the wall;
sat, at saturation.

1. INTRODUCTION

IT WAS Nusselt [1] who first, in 1916, analytically treated the laminar condensation of quiescent vapours on flat vertical surfaces and horizontal cylinders. From that time, being of direct technical importance, the problem of vapour condensation on horizontal cylinders has received a lot of attention; and many workers modified the simple theory (Sparrow and Gregg [2], Chen [3], etc.). An important factor related to that problem and greatly influencing the mechanism of heat transfer is the velocity of the oncoming vapour. The vapour experiences shear forces on the liquid film; moreover a pressure gradient is generated in that film. This causes thinning of the condensate film on the forward half of the cylindrical surface and hence reduces its thermal resistance. Shekriladze and Gomelauri [4] analysed this problem. In their analysis, they ignored in the condensate layer pressure, inertia and gravity forces, energy convection and condensate subcooling. By equating shear stress at liquid–vapour interface to change in momentum flux of the condensing vapour, they managed to eliminate the equation of motion in the vapour phase. Denny and Mills [5] made similar approximations, and they included gravity forces in liquid layer and condensate subcooling in their energy balance. Fujii *et al.* [6] considered the equation of motion in the vapour boundary layer. However, they approximated the velocity profile in that layer by a quadratic formula, and still ignored in the condensate film inertia and pressure forces, energy convection and liquid subcooling. Schmal [7] treated the same set of equations in [6] but he eliminated gravity forces, and still ignored liquid convection and subcooling.

Such approximations may be justified in many cases, but they cannot be generalized over the whole range of the governing parameters. Thus, a need arises for a method for solving the full two phase boundary-layer equations. The work presented in this paper is devoted towards this aim. Solutions, based on this method, for numerical values covering a wide range of the governing parameters are presented and discussed.

2. FORMULATION OF THE PROBLEM

2.1. *Description of the model*

The physical model is shown in orthogonal curvilinear coordinates in Fig. 1(a). A condensate film flows around a horizontal cylindrical surface. The condensate film is surrounded by a vapour boundary layer. Outside the vapour layer, the flow is ideal. The undisturbed vapour velocity and the force of gravity have the same direction. The x-axis is along the liquid–vapour interface, and the point of origin is the upper intersection between the liquid–vapour interface and the axis of symmetry. The equivalent model in cartesian coordinates is shown in Fig. 1(b).

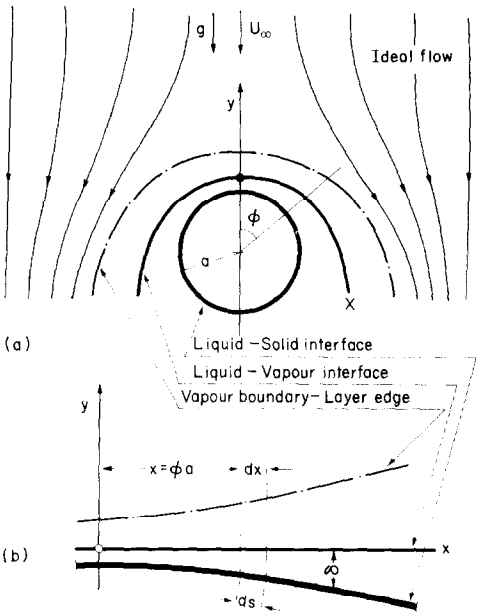

FIG. 1. (a) Model in orthogonal curvilinear co-ordinates; (b) Equivalent model in cartesian co-ordinates.

2.2. *Assumptions*

The following assumptions have been made:

(1) Physical properties are constant.
(2) Surface tension forces are insignificant.
(3) Thicknesses of liquid and vapour layers are small compared with tube radius.
(4) Vapour velocity components along and perpendicular to the liquid–vapour interface have insignificant effects on velocity and pressure distributions in the ideal flow region.
(5) Fluid motion in liquid and vapour layers is laminar up to the separation point.
(6) Undisturbed vapour velocity is steady and uniform and has a low Mach number.
(7) Vapour is initially pure, dry and saturated.
(8) Temperature variations at liquid–vapour interface between liquid and vapour phases are insignificant.
(9) Change in momentum flux at liquid–vapour interface perpendicular to that interface due to change in fluid velocity by condensation has negligible effect on pressure distribution in the liquid film.
(10) Steady state is achieved.
(11) Viscous dissipation is ignored.
(12) Wall surface temperature is uniform.

2.3. *Boundary-layer equations*

In liquid layer. Conservation of mass, momentum and energy in liquid boundary layer is expressed respectively by

$$\frac{\partial u_l}{\partial x} + \frac{\partial v_l}{\partial y} = 0 \qquad (1)$$

$$u_l\frac{\partial u_l}{\partial x}+v_l\frac{\partial u_l}{\partial y}=g\left(\frac{\rho_l-\rho_v}{\rho_l}\right)\sin\left(\frac{x}{a}\right)$$
$$-\frac{1}{\rho_l}\frac{\mathrm{d}p}{\mathrm{d}x}+\nu_l\frac{\partial^2 u_l}{\partial y^2} \quad (2)$$

$$u_l\frac{\partial T_l}{\partial x}+v_l\frac{\partial T_l}{\partial y}=\alpha_l\frac{\partial^2 T_l}{\partial y^2}. \quad (3)$$

In vapour layer. Similarly in the vapour boundary layer

$$\frac{\partial u_v}{\partial x}+\frac{\partial v_v}{\partial y}=0 \quad (4)$$

$$u_v\frac{\partial u_v}{\partial x}+v_v\frac{\partial u_v}{\partial y}=-\frac{1}{\rho_v}\frac{\mathrm{d}p}{\mathrm{d}x}+\nu_v\frac{\partial^2 u_v}{\partial y^2} \quad (5)$$

$$T_v=T_{\mathrm{sat}}=\text{constant}. \quad (6)$$

2.4. *Boundary and interfacial conditions*

At liquid–solid interface (y = $-\delta$).

$$u_l=0 \quad (7)$$

$$v_l=0 \quad (8)$$

$$T_l=T_w \quad (9)$$

At liquid–vapour interface (y = 0).

$$u_l=u_v \quad (10)$$

$$\rho_l v_l=\rho_v v_v \quad (11)$$

$$\mu_l\frac{\partial u_l}{\partial y}=\mu_v\frac{\partial u_v}{\partial y} \quad (12)$$

$$T_l=T_v. \quad (13)$$

At vapour boundary-layer edge. At the edge of the vapour boundary layer, the velocity component in the x direction approaches the velocity in the main stream asymptotically. The main stream velocity is obtained from the ideal flow theory. This may be expressed as: at $y=\infty$

$$u_v=2U_\infty\sin\left(\frac{x}{a}\right). \quad (14)$$

2.5. *Energy balance*

From an energy balance in the condensate layer

$$q_w\,\mathrm{d}s=\frac{\mathrm{d}Q}{\mathrm{d}x}\mathrm{d}x. \quad (15)$$

Within the accuracy of the boundary layer assumptions, the approximation $\mathrm{d}s\approx\mathrm{d}x$ may be made. Equation (15) yields

$$k_l\left(\frac{\partial T_l}{\partial y}\right)_{y=-\delta}=\frac{\mathrm{d}}{\mathrm{d}x}$$
$$\left[\int_{y=-\delta}^{0}\{\rho_l L+\rho_l c_l(T_{\mathrm{sat}}-T_l)\}u_l\,\mathrm{d}y\right] \quad (16)$$

3. MATHEMATICAL ANALYSIS

3.1. *In liquid layer*

The continuity equation in the liquid layer is satisfied by introducing a stream function ψ_l related to the velocity components by

$$u_l=\frac{\partial\psi_l}{\partial y} \quad (17)$$

$$v_l=-\frac{\partial\psi_l}{\partial x}. \quad (18)$$

The pressure gradient in the liquid layer is obtained from the theory of ideal flow, or

$$\frac{\mathrm{d}p}{\mathrm{d}x}=-\frac{2\rho_v U_\infty^2}{a}\sin\left(\frac{2x}{a}\right). \quad (19)$$

Substituting in equation (2) gives

$$\frac{\partial\psi_l}{\partial y}\frac{\partial^2\psi_l}{\partial x\partial y}-\frac{\partial\psi_l}{\partial x}\frac{\partial^2\psi_l}{\partial y^2}$$
$$=g\left(\frac{\rho_l-\rho_v}{\rho_l}\right)\sin\left(\frac{x}{a}\right)$$
$$+\frac{2\rho_v U_\infty^2}{a\rho_l}\sin\left(\frac{2x}{a}\right)$$
$$+\nu_l\frac{\partial^3\psi_l}{\partial y^3}. \quad (20)$$

Equation (20) may be transformed into a dimensionless form by introducing the following dimensionless quantities:

$$\psi_l^*=\frac{\psi_l}{\nu_l} \quad (21)$$

(dimensionless stream function)

$$\phi=\frac{x}{a} \quad (22)$$

(dimensionless distance in x direction)

$$Y=\frac{y}{\delta} \quad (23)$$

(dimensionless distance in y direction).

Now

$$\frac{\partial^m\psi_l}{\partial y^m}=\frac{\nu_l}{a^m\Delta^m}\frac{\partial^m\psi_l^*}{\partial Y^m}$$

and

$$\frac{\partial^2\psi_l}{\partial x\,\partial y}=\frac{\nu_l}{a^2}\left[\frac{1}{\Delta}\frac{\partial^2\psi_l^*}{\partial\phi\,\partial Y}-\frac{1}{\Delta^2}\frac{\mathrm{d}\Delta}{\mathrm{d}\phi}\frac{\partial\psi_l^*}{\partial Y}\right]$$

where

$$\Delta=\frac{\delta}{a} \quad (24)$$

(dimensionless condensate thickness).

Substituting in equation (20) gives

$$\Delta\frac{\partial\psi_l^*}{\partial Y}\frac{\partial^2\psi_l^*}{\partial\phi\,\partial Y}-\frac{\mathrm{d}\Delta}{\mathrm{d}\phi}\left(\frac{\partial\psi_l^*}{\partial Y}\right)^2$$
$$-\Delta\frac{\partial\psi_l^*}{\partial\phi}\frac{\partial^2\psi_l^*}{\partial Y^2}=N_{lg}\Delta^3\sin(\phi) \quad (25)$$
$$+N_{lp}\Delta^3\sin(2\phi)+\frac{\partial^3\psi_l^*}{\partial Y^3}$$

where

$$N_{lg} = \frac{ga^3(\rho_l - \rho_v)}{v_l^2 \rho_l} = \frac{Ga}{8}\left(\frac{R_d - 1}{R_d}\right) \tag{26}$$

$$N_{lp} = \frac{2a^2 \rho_v U_\infty^2}{v_l^2 \rho_l} = \frac{Re^2}{2R_v^2 R_d} \tag{27}$$

and

$$Re = \frac{2aU_\infty}{v_v} \text{(Reynolds number)} \tag{28}$$

$$Ga = \frac{(2a)^3 g}{v_l^2} \text{(Galileo number)} \tag{29}$$

$$R_d = \frac{\rho_l}{\rho_v} \text{ (density ratio)} \tag{30}$$

$$R_v = \frac{v_l}{v_v} \tag{31}$$

(kinematic viscosity ratio).

Let the dimensionless stream function ψ_l^* be expressed by an infinite odd series in ϕ (Blasius series) [8], or

$$\psi_l^* = \sum_{n=0}^{\infty} F_{2n+1} \phi^{2n+1}. \tag{32}$$

The coefficient F_{2n+1} is a function of Y only. Now

$$\frac{\partial^m \psi_l^*}{\partial Y^m} = \sum_{n=0}^{\infty} F_{2n+1}^{(m)} \phi^{2n+1}$$

$$\frac{\partial \psi_l^*}{\partial \phi} = \sum_{n=0}^{\infty} (2n+1) F_{2n+1} \phi^{2n} - \frac{Y \, d\Delta}{\Delta \, d\phi} \sum_{n=0}^{\infty} F'_{2n+1} \phi^{2n+1}$$

$$\frac{\partial^2 \psi_l^*}{\partial \phi \partial Y} = \sum_{n=0}^{\infty} (2n+1) F'_{2n+1} \phi^{2n} - \frac{Y \, d\Delta}{\Delta \, d\phi} \sum_{n-0}^{\infty} F''_{2n+1} \phi^{2n+1}.$$

Primes denote differentiation with respect to Y, and $F_{2n+1}^{(m)}$ is the mth derivative of F_{2n+1}.

Let the dimensionless condensate layer thickness Δ be represented by an infinite even series in ϕ (symmetrical about the y axis), or

$$\Delta = \sum_{n=0}^{\infty} b_{2n} \phi^{2n}. \tag{33}$$

Substituting in equation (25) and replacing sin (ϕ) and sin (2ϕ) by infinite power series in ϕ give an equation which contains terms each of them is a multiplication of a number of infinite series. Carrying out the multiplication and rearranging give

$$\sum_{n=0}^{\infty} \left\{ F'''_{2n+1} + \sum_{j=0}^{n} \left[b_{2n-2j} \sum_{i=0}^{j} \left((2i+1) F_{2i+1} F''_{2j+1-2i} + (2n-2j-1-2i) F'_{2i+1} F'_{2j+1-2i} \right) \right] + W_{2n+1} \right\} \phi^{2n+1} = 0. \tag{34}$$

W_{2n+1} is a constant defined by

$$W_{2n+1} = N_{lg} \varepsilon_{2n+1}(1) + N_{lp} \varepsilon_{2n+1}(2) \tag{35}$$

and

$$\varepsilon_{2n+1}(m) = \sum_{j=0}^{n} \left\{ \frac{(-)^{n-j} (m)^{2n+1-2j}}{(2n+1-2j)!} \sum_{i=0}^{j} \left[b_{2j-2i} \sum_{r=0}^{i} (b_{2r} b_{2i-2r}) \right] \right\}. \tag{36}$$

Equation (34) is satisfied at all values of ϕ, hence the coefficient of ϕ^{2n+1} must be zero for all values of n. Thus,

$$F'''_{2n+1} + \left\{ \sum_{j=0}^{n} \left[b_{2n-2j} \sum_{i=0}^{j} \left((2i+1) F_{2i+1} F''_{2j+1-2i} + (2n-2j-1-2i) F'_{2i+1} F'_{2j+1-2i} \right) \right] \right\} + W_{2n+1} = 0. \tag{37}$$

Equation (37) represents an infinite set of ordinary differential equations. The individual equations are obtained by substituting $n = 0, 1, 2, 3 \ldots$ etc. Substituting and rearranging give

for $n = 0$:

$$F'''_1 + \{b_0 [F_1 F''_1 - (F'_1)^2]\} + W_1 = 0 \tag{38}$$

$$\varepsilon_1(1) = b_0^3 \tag{39}$$

$$\varepsilon_1(2) = 2b_0^3 \tag{40}$$

for $n = 1$:

$$F'''_3 + \{b_0 [F_1 F''_3 - 4F'_1 F'_3 + 3F''_1 F_3] + D_3\} + W_3 = 0 \tag{41}$$

$$D_3 = b_2 [F_1 F''_1 + (F'_1)^2] \tag{42}$$

$$\varepsilon_3(1) = b_0^2 (3b_2 - \tfrac{1}{6} b_0) \tag{43}$$

$$\varepsilon_3(2) = b_0^2 (6b_2 - \tfrac{4}{3} b_0) \tag{44}$$

for $n \geqslant 2$:

$$F'''_{2n+1} + \{b_0 [F_1 F''_{2n+1} - (2n+2) F'_1 F'_{2n+1} + (2n+1) F''_1 F_{2n+1}] + D_{2n+1}\} + W_{2n+1} = 0 \tag{45}$$

where

$$D_{2n+1} = \sum_{j=0}^{n-1} \left[b_{2n-2j} \sum_{i=0}^{j} \left((2i+1) F_{2i+1} F''_{2j+1-2i} + (2n-2j-1-2i) F'_{2i+1} F'_{2j+1-2i} \right) \right] + b_0 \sum_{i=1}^{n-1} \left((2i+1) F_{2i+1} F''_{2n+1-2i} - (2i+1) F'_{2i+1} F'_{2n+1-2i} \right). \tag{46}$$

If the inertia term is ignored in the equation of motion, the term between brackets in equation (37) disappears; the set of equations becomes then

$$F'''_{2n+1} + W_{2n+1} = 0 \quad (n \geqslant 0). \tag{47}$$

3.2. *In vapour layer*

The momentum equation in the vapour layer may be treated in a similar manner using the following substitutions:

$$u_v = \frac{\partial \psi_v}{\partial y} \tag{48}$$

$$v_v = -\frac{\partial \psi_v}{\partial x} \tag{49}$$

$$\psi_v^* = \frac{\psi_v}{\nu_v} = \sum_{n=0}^{\infty} f_{2n+1}\,\phi^{2n+1} \tag{50}$$

$$N_{vp} = \frac{2a^2 U_\infty^2}{\nu_v^2} = \frac{Re^2}{2} \tag{51}$$

The corresponding ordinary differential equations are:

for $n = 0$:

$$f_1''' + \{b_0[f_1 f_1'' - (f_1')^2]\} + w_1 = 0 \tag{52}$$

for $n = 1$

$$f_3''' + \{b_0[f_1 f_3'' - 4f_1' f_3 + 3f_1'' f_3] + d_3\} + w_3 = 0 \tag{53}$$

$$d_3 = b_2[f_1 f_1'' + (f_1')^2] \tag{54}$$

for $n \geqslant 2$:

$$f_{2n+1}''' + \{b_0[f_1 f_{2n+1}'' - (2n+2) f_1' f_{2n+1}' + (2n+1) f_1'' f_{2n+1}] + d_{2n+1}\} + w_{2n+1} = 0 \tag{55}$$

$$d_{2n+1} = \sum_{j=0}^{n-1}\left[b_{2n-2j} \times \sum_{i=0}^{j} ((2i+1) f_{2i+1} f_{2j+1-2i}'' + (2n-2j-1-2i) f_{2i+1}' f_{2j+1-2i}')\right] + b_0 \sum_{i=1}^{n-1} ((2i+1) f_{2i+1} f_{2n+1-2i}'' - (2i+1) f_{2i+1}' f_{2n+1-2i}') \tag{56}$$

f_{2n+1} is a function of Y only and w_{2n+1} is a constant defined by

$$w_{2n+1} = N_{vp}\,\varepsilon_{2n+1}(2) \quad \text{for} \quad n \geqslant 0. \tag{57}$$

3.3. *Energy equation in liquid layer*

Substituting in equation (3) gives

$$\frac{\partial \psi_l}{\partial y}\frac{\partial T_l}{\partial x} - \frac{\partial \psi_l}{\partial x}\frac{\partial T_l}{\partial y} = \alpha_l \frac{\partial^2 T_l}{\partial y^2} \tag{58}$$

Let

$$\theta_l = \frac{T_l - T_{sat}}{T_w - T_{sat}}. \tag{59}$$

Substituting in equation (58) and rearranging give

$$\Delta \frac{\partial \psi_l^*}{\partial Y}\frac{\partial \theta_l}{\partial \phi} - \Delta \frac{\partial \psi_l^*}{\partial \phi}\frac{\partial \theta_l}{\partial Y} = \frac{1}{Pr}\frac{\partial^2 \theta_l}{\partial Y^2} \tag{60}$$

Let

$$\theta_l = \sum_{n=0}^{\infty} A_{2n}\,\phi^{2n}. \tag{61}$$

A_{2n} is a function of Y only. Differentiating, substituting and rearranging yield the following set of ordinary differential equations:

for $n = 0$:

$$A_0'' + Pr\,(b_0 F_1 A_0') = 0 \tag{62}$$

for $n \geqslant 1$:

$$A_{2n}'' + Pr[b_0(F_1 A_{2n}' - 2nF_1' A_{2n}) + E_{2n}] = 0 \tag{63}$$

where

$$E_{2n} = \sum_{j=1}^{n}\left\{ A_{2n-2j}' \times \sum_{i=0}^{j}[(2j+1-2i) b_{2i} F_{2j+1-2i}] - (2n-2j) A_{2n-2j} \times \sum_{i=0}^{j} (b_{2i} F_{2j+1-2i}')\right\}. \tag{64}$$

If energy transport by convection is ignored, the terms between brackets disappear. The set of equations becomes then

$$A_{2n}'' = 0 \quad (n \geqslant 0). \tag{65}$$

3.4. *Boundary and interfacial conditions*

At liquid–solid interface ($Y = -1$).

$$F_{2n+1}'(-1) = 0 \tag{66}$$

$$F_{2n+1}(-1) = 0 \tag{67}$$

$$A_{2n}(-1) = 1 \quad \text{for} \quad (n = 0) \tag{68}$$

and

$$A_{2n}(-1) = 0 \quad \text{for} \quad (n > 0). \tag{69}$$

At liquid–vapour interface ($Y = 0$)

$$f_{2n+1}'(0) = R_v F_{2n+1}'(0) \tag{70}$$

$$f_{2n+1}(0) = R_d R_v F_{2n+1}(0) \tag{71}$$

$$f_{2n+1}''(0) = R_d R_v^2 F_{2n+1}''(0) \tag{72}$$

$$A_{2n}(0) = 0. \tag{73}$$

At $Y = \infty$

From equation (14)

$$\left(\frac{\partial \psi_v^*}{\partial Y}\right)_{Y=\infty} = Re\,\Delta \sin\phi \tag{74}$$

Substituting for Δ from equation (33), replacing sin ϕ by an infinite series in ϕ and carrying out the multiplication give

$$f_{2n+1}'(\infty) = Re \sum_{j=0}^{n} \frac{(-)^j}{(2j+1)!} b_{2n-2j}. \tag{75}$$

3.5. *Energy balance*

Re-arranging equation (16) in a dimensionless

form and carrying out the involved series multiplication yield the following equation:

$$A'_{2n}(-1)+\sum_{j=0}^{n}\left\{(2j+1)b_{2n-2j}\left(\frac{Pr}{Ph}F_{2j+1}(0)+PrI_{2j+1}\right)\right\}=0 \quad (76)$$

where

$$Ph=\frac{c_1(T_{sat}-T_w)}{L}\ \text{(phase change number)} \quad (77)$$

$$I_{2n+1}=\int_{Y=-1}^{0}P_{2n+1}\,dY \quad (78)$$

and

$$P_{2n+1}=\sum_{j=0}^{n}A_{2n-2j}F'_{2j+1}. \quad (79)$$

P_{2n+1} a function of Y and I_{2n+1} is a constant.

for $n=0$:

$$b_0=-\frac{A'_0(-1)}{\frac{Pr}{Ph}F_1(0)+PrI_1} \quad (80)$$

for $n>0$:

$$b_{2n}=-\frac{A'_{2n}(-1)+\sum_{j=1}^{n}\left\{(2j+1)b_{2n-2j}\left[\frac{Pr}{Ph}F_{2j+1}(0)+PrI_{2j+1}\right]\right\}}{\frac{Pr}{Ph}F_1(0)+PrI_1} \quad (81)$$

4. HEAT-TRANSFER RELATIONSHIPS

$$q_w=k_l\left(\frac{\partial T_l}{\partial y}\right)_{y=-\delta}=h(T_{sat}-T_w) \quad (82)$$

Substituting and re-arranging give

$$(Nu)_\phi=\left(\frac{2ah}{k_l}\right)_\phi=-2\sum_{n=0}^{\infty}\gamma_{2n}\phi^{2n} \quad (83)$$

where

$$\gamma_0=\frac{A'_0(-1)}{b_0} \quad (84)$$

$$\gamma_{2n}=\frac{1}{b_0}\left[A'_{2n}(-1)-\sum_{j=1}^{n}b_{2j}\gamma_{2n-2j}\right]$$

for $n>0$. (85)

Equation (83) gives the local value of the Nusselt number. The validity of this equation is up to the point where flow separation takes place.

If flow separation does not occur, equation (83) may be integrated to give the mean Nusselt number Nu_m. This yields

$$Nu_m=\frac{1}{\pi}\int_{\phi=0}^{\pi}(Nu)_\phi\,d\phi=-2\sum_{n=0}^{\infty}\frac{\gamma_{2n}}{2n+1}\pi^{2n} \quad (86)$$

5. NOTE ON THE PROCEDURE OF COMPUTATION

A set of 3 ordinary differential equations with the corresponding boundary and interfacial conditions and an algebraic equation (emerging from the energy balance) exists for each value of n. Since each set is independent of the other sets for higher values of n, the solution was carried out step by step starting with $n=0$. The two equations of motion for each n were solved simultaneously independent of the energy equation. This can be done provided that the coefficient b_{2n} is known. Since b_{2n} is the outcome of the solution, its value was initially assumed and checked at a later stage. A numerical solution based on the assumed value of b_{2n} yielded the functions F_{2n+1}, f_{2n+1} and their higher derivatives at different mesh points. These values were fed in the energy equation and a solution of the latter was obtained. The energy balance equation provided the check for the assumed value of b_{2n}, and if it was necessary another guess was made and the procedure was repeated.

The local Nusselt number and the condensate layer thickness at the forward stagnation point are yielded from the first set of equations corresponding to $n=0$. Three sets are enough for an accurate evaluation of the local Nusselt number up to $\phi=1.0$, and eight sets were considered up to $\phi=1.8$. Solutions for evaluating the mean Nusselt number and for predicting the position of flow separation ($\phi>2.0$) were carried out with eight and twelve sets respectively.

Since the solution corresponding to each n is an input to the equations of higher n, a high degree of accuracy is essential. This was checked by varying the number of intervals in liquid and vapour layers. Limited space does not allow more elaboration.

6. NUMERICAL RESULTS

6.1. *Quiescent vapour* (Re = 0)

The case of a quiescent vapour is treated as a special case of the general solution by substituting $Re=0$. Numerical results are presented for steam condensing at pressures 0.1, 1 and 10 atm on a tube of about 20 mm dia with temperature difference ($T_{sat}-T_w$) of about 1, 5 and 20 C. The values of the governing dimensionless parameters are given in Table 1 (Data No. 1–9). The other computed values in Table 1 are for the condensation of a vapour metal (Date No. 10–12) and of vapours of viscous liquids (Data No. 13–15). The computed values of the local Nusselt number Nu_0 and the local

Table 1. Comparison between Nusselt theory and present work with $Re = 0$

Fluid	R_d	R_v	Ga	Pr	Ph	Δ_0	$Nu_0^\dagger$	$Nu_0^\ddagger$	$Nu_m^\dagger$	$Nu_m^\ddagger$	Data No.
Water ($p = 0.1$ atm)	1.45×10^4	3.76×10^{-3}	2.77×10^8	3.7	2×10^{-3}	2.62×10^{-3}	765	765	618	613	1
					10^{-2}	3.91×10^{-3}	512	511	414	410	2
					4×10^{-2}	5.53×10^{-3}	363	362	294	290	3
Water ($p = 1$ atm)	1.60×10^3	1.40×10^{-2}	1.02×10^9	1.74	2×10^{-3}	2.28×10^{-3}	877	877	709	704	4
					10^{-2}	3.41×10^{-3}	586	586	475	471	5
					4×10^{-2}	4.84×10^{-3}	415	415	337	333	6
Water ($p = 10$ atm)	1.73×10^2	5.75×10^{-2}	2.96×10^9	1.0	2×10^{-3}	2.01×10^{-3}	995	997	805	800	7
					10^{-2}	3.01×10^{-3}	665	666	538	535	8
					4×10^{-2}	4.28×10^{-3}	469	471	381	378	9
Liquid metal ($Pr \ll 1$)	3.4×10^3	3.2×10^{-2}	10^9	5×10^{-3}	2×10^{-3}	1.08×10^{-2}	185	202	154	162	10
					10^{-2}	1.95×10^{-2}	103	135	87.4	108	11
					4×10^{-2}	3.57×10^{-2}	56.4	95.5	48.2	76.7	12
Viscous liquids ($Pr \gg 1$)	10	0.1	10^8	10	1	1.25×10^{-2}	173	161	141	129	13
				10^2	1	6.85×10^{-3}	315	286	255	229	14
				10^3	1	3.83×10^{-3}	564	508	456	408	15

† Based on present work with $Re = 0$.
‡ Based on Nusselt theory.

dimensionless layer thickness Δ_0 at the forward stagnation point and the mean Nusselt number Nu_m are given in Table 1. Comparison is made between the values based on the present work $(Nu_0)^\dagger$ and $(Nu_m)^\dagger$ and the corresponding values based on the Nusselt theory $(Nu_0)^\ddagger$ and $(Nu_m)^\ddagger$. The tabulated values in Table 1 based on the Nusselt theory are evaluated from the expressions

$$(Nu_0)^\ddagger_\ddagger = \left[\frac{2\,Ga\,Pr}{3\,Ph}\right]^{0.25} \tag{87}$$

and

$$(Nu_m)^\ddagger_\ddagger = 0.725\left[\frac{Ga\,Pr}{Ph}\right]^{0.25} \tag{88}$$

Agreement exists between the Nusselt theory and the present work with water at the given pressures and the given values of the phase change number Ph. However, the Nusselt theory overestimates the local and mean values of the Nusselt number in the liquid metal case and underestimates them in the case of a viscous liquid when $Ph = 1.0$. The values of Nu_0 and Nu_m based on the Nusselt theory are respectively 69% and 59% higher with Data No. 12 and 9% and 10% lower with Data No. 14 compared with the corresponding values based on the present work. Data No. 12 for a liquid metal and Data No. 14 for a viscous condensate are analysed further in Table 2. The assumptions in the Nusselt theory are examined separately and together. It is seen in Table 2, that for the liquid metal case the elimination of the convection term, as expected, has no effect on the Nusselt number. Since in this case $Ph \ll 1.0$, ignoring subcooling in the condensate is also ineffective. However, ignoring inertial forces in the condensate layer leads to an increase in the local Nusselt number Nu_0 and the mean Nusselt number Nu_m by

Table 2. Effects of ignoring inertia forces, energy convection, condensate subcooling and shear forces at interface on Nusselt number ($Re = 0$)

	Liquid metal Data No. 12		Viscous liquid Data No. 14	
	Nu_0	Nu_m	Nu_0	Nu_m
Present work	56.4	48.2	315	255
A	73.3	59.4	316	256
B	56.2	48.1	299	243
C	55.9	47.8	298	242
D	67.3	59.7	317	257
$A+B+C+D$	95.5	77.3	278	225
Nusselt theory	95.5	76.7	286	229

Ignored in condensate layer: A, inertia forces; B, energy convection; C, condensate subcooling in energy balance; D, shear forces at liquid-vapour interface.

30% and 23% respectively. Meanwhile, ignoring the shear forces at the liquid–vapour interface increases Nu_0 and Nu_m by 19% and 24% respectively. The velocity distribution at $\phi = 1$ for that particular case is shown in Fig. 2. It is seen in that figure that the maximum value of the liquid velocity u_l^* ($= u_l a/\nu_l$) for the full solution is attained at $Y = -0.59$ (nearer to the wall rather than to the liquid–vapour interface). The liquid–vapour interface velocity amounts only to 25% of the maximum value. The velocity distributions based on ignoring the inertia term in the condensate $[u_l^*]_A$, the shear forces at the liquid–vapour interface $[u_l^*]_D$ and when meeting all the assumptions in the Nusselt theory $[u_l^*]_{A\ldots D}$ are also shown in Fig. 2.

Ignoring the inertial forces in the condensate layer and the shear forces at the interface with Data No. 14 ($Pr = 100$, $Ph = 1$) have insignificant effect on the value of the Nusselt number. However, eliminating convection in the energy equation or ignoring liquid

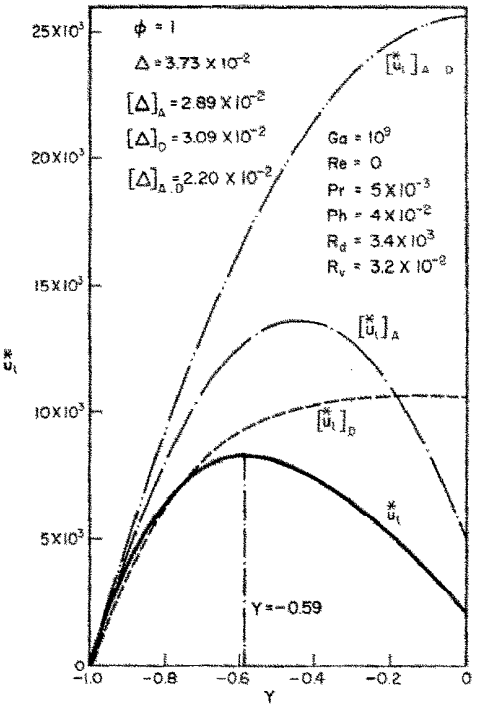

FIG. 2. Velocity distribution in condensate layer.

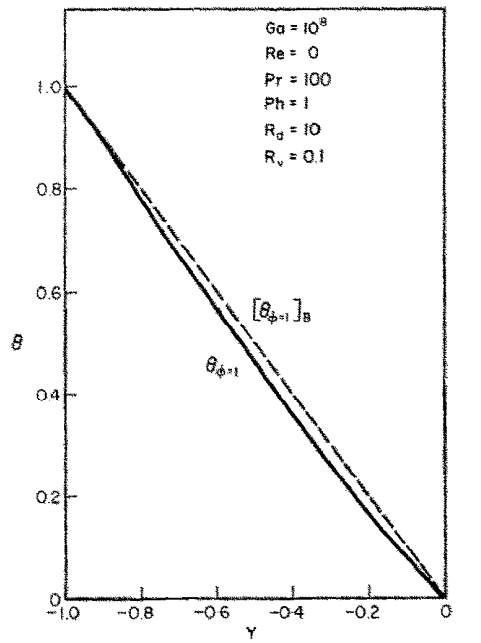

FIG. 3. Temperature distribution in condensate layer.

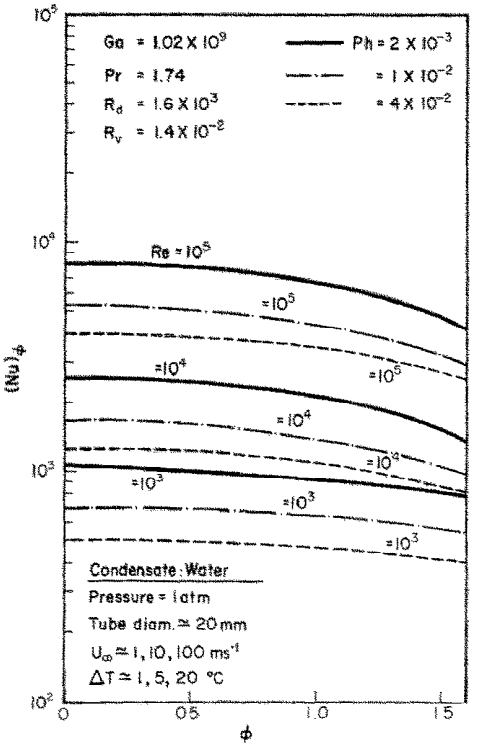

FIG. 4. Local Nusselt number distribution for water at 1 atm.

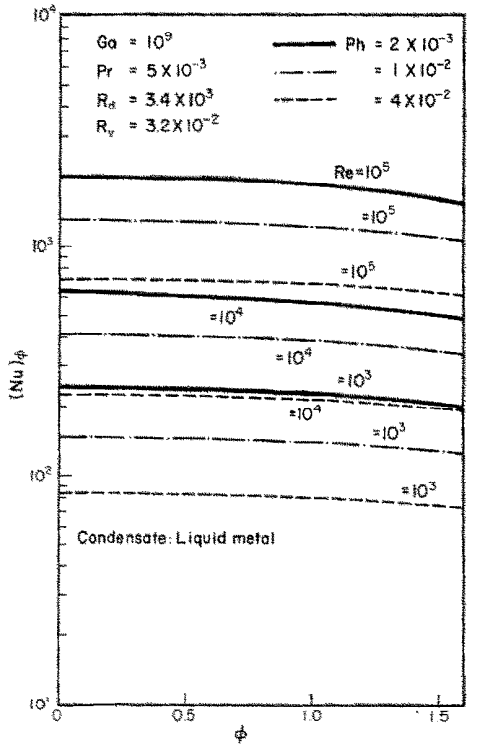

FIG. 5. Local Nusselt number distribution for a liquid metal.

subcooling leads to a reduction of 5% in Nu_0 and Nu_m. The dimensionless temperature distribution in the condensate layer at $\phi = 1$ is shown for that particular case in Fig. 3. The difference between the temperature distribution $\theta_{\phi=1}$ corresponding to the full solution and the linear distribution $[\theta_{\phi=1}]_B$ based on ignoring liquid convection is not very remarkable. In both cases (Data No. 12 and Data No. 14), when all the assumptions in the Nusselt theory were met [case $(A+B+C+D)$], agreement between the computed results based on this analysis and those calculated from equations (87) and (88) is achieved.

Table 3. Effect of Reynolds number on Nusselt number and boundary layer thickness (water)

Pressure	Re	Δ_0	Nu_0	Nu_m	Data No.
0.1 atm	1.4×10^2	2.46×10^{-3}	812		1
	1.4×10^3	1.34×10^{-3}	1491		
	1.4×10^4	4.35×10^{-4}	4597		
	1.4×10^2	3.61×10^{-3}	555	434	2
	1.4×10^3	1.94×10^{-3}	1032		
	1.4×10^4	6.29×10^{-4}	3182		
	1.4×10^2	4.85×10^{-3}	414	322	3
	1.4×10^3	2.33×10^{-3}	863	544†	
	1.4×10^4	7.47×10^{-4}	2688		
1 atm	10^3	1.94×10^{-3}	1035		4
	10^4	7.83×10^{-4}	2553		
	10^5	2.49×10^{-4}	8037		
	10^3	2.90×10^{-3}	691		5
	10^4	1.21×10^{-3}	1652		
	10^5	3.85×10^{-4}	5194		
	10^3	3.92×10^{-3}	512	383	6
	10^4	1.59×10^{-3}	1264		
	10^5	5.05×10^{-4}	3977		
10 atm	7×10^3	1.32×10^{-3}	1520		7
	7×10^4	4.45×10^{-4}	4493		
	7×10^5	1.41×10^{-4}	14196		
	7×10^3	2.08×10^{-3}	961		8
	7×10^4	7.21×10^{-4}	2778		
	7×10^5	2.28×10^{-4}	8774		
	7×10^3	2.96×10^{-3}	678		9
	7×10^4	1.03×10^{-3}	1942		
	7×10^5	3.27×10^{-4}	6135		

† Separation starts near backward stagnation point.

Table 4. Effect of Reynolds number on Nusselt number and boundary-layer thickness (liquid metal)

Re	Δ_0	Nu_0	Nu_m	Data No.
10^3	8.19×10^{-3}	244	192	
10^4	3.15×10^{-3}	634	466	10
10^5	1.00×10^{-3}	1999	1465	
10^3	1.34×10^{-2}	150	122	
10^4	4.85×10^{-3}	413	329	11
10^5	1.54×10^{-3}	1303	1038	
10^3	2.39×10^{-2}	84.2	70.5	
10^4	8.90×10^{-3}	225	190	12
10^5	2.82×10^{-3}	711	598	

Table 5. Effect of Reynolds number on Nusselt number and boundary-layer thickness (viscous liquids)

Re	Δ_0	Nu_0	Data No.
10^3	7.18×10^{-3}	298	
10^4	2.36×10^{-3}	906	13
10^5	7.46×10^{-4}	2865	
10^3	3.41×10^{-3}	628	
10^4	1.10×10^{-3}	1943	14
10^5	3.48×10^{-4}	6144	
10^3	1.59×10^{-3}	1342	
10^4	5.08×10^{-4}	4200	15
10^5	1.61×10^{-4}	13279	

6.2. *Flowing vapour* ($\mathrm{Re}\neq0$)

Computations were made at different values of the Reynolds number and the values given in Table 1 for the parameters Ga, Pr, Ph, R_d and R_v. The same data numbers are still used to refer to the values of the five parameters $Ga\ldots Rv$ when calculations were made with $Re\neq0$. The computed local values of the Nusselt number Nu_0 and condensate thickness Δ_0 are given in Tables 3–5. The values of the mean Nusselt number, as long as flow separation does not occur, are also present in the tables. The variation of the local Nusselt number with ϕ at the different values of Re is shown in Figs. 4–6 for the cases of water at 1 atm, a liquid metal and a viscous liquid respectively. The general trend in the figures is that the local Nusselt number distribution is flatter at the lower values of the Reynolds number and attains fairly similar profiles with increasing Reynolds

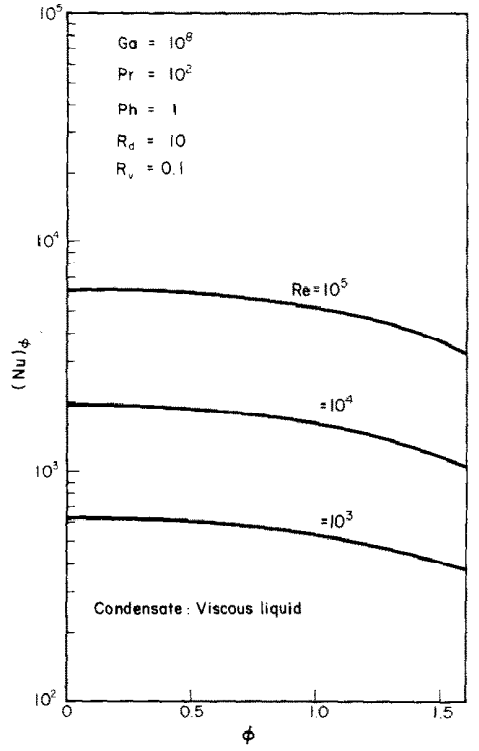

FIG. 6. Local Nusselt number distribution for a viscous condensate.

number. In Fig. 7, the ratio $[(Nu)_{Re\neq 0}/(Nu)_{Re=0}]$ is plotted against the Reynolds number for condensing steam at 1 atm. Three distinct regions are clear in Fig. 7. At low Reynolds number, the condensate layer is gravity controlled. At sufficiently high Reynolds number, the condensate layer is vapour-shear controlled. The dependence of the local Nusselt number Nu_0 at the forward stagnation point fulfils in that region the following relationship

$$Nu_0 \propto Re^{0.5}.$$

In the intermediate region, where both gravity forces and vapour-shear forces are influential, a relation similar to that in the vapour-shear controlled region does not exist.

Because the profile of the local Nusselt number distribution at the forward half of the cylindrical surface is nearly identical at high Reynolds numbers, and since most of the condensation takes place at that half, the ratio $[Nu_m/Nu_0]$ may be fairly constant in the vapour-shear controlled region. The value of the mean Nusselt number in that region may still be expressed by the relation

$$Nu_m \propto Re^{0.5}.$$

Similar conclusion has been reached in [4, 6, 7].

It is clear from Fig. 7, that the threshold value of the Reynolds number at which vapour-shear forces become influential increases with increasing steam pressure.

Data No. 5 are further examined for a quiescent and a flowing vapour ($Re = 0, 10^4$). While keeping the other parameters unchanged at their value in the initial state (i), one of them has been varied and the ratio $[Nu_0/(Nu_0)_i]$ is plotted in Fig. 8 against the ratio of that parameter to its initial value [parameter/(parameter)$_i$]. Comparing the two cases in Fig. 8 shows the difference in the functional dependence of the Nusselt number on the governing parameters between the case of a gravity controlled- and that of a vapour-shear controlled condensate layer.

7. FLOW SEPARATION

The criterion for flow separation at the solid wall given by $(\partial u_l/\partial y)_{y=-\delta} = 0$ leads to

$$\sum_{n=0}^{\infty} F''_{2n+1}(-1)\phi^{2n+1} = 0. \tag{89}$$

Equation (89) has been examined in case of Data No. 4 at different Reynolds numbers. When $Re = 10^2$ flow separation in the condensate layer does not occur. Examining the velocity distribution in the vapour phase shows that the vapour changes its direction of motion at $\phi \simeq 2.4$ (see Fig. 9). The region of reversed flow motion lies entirely in the vapour layer. At $Re = 10^3$ flow seperation in the condensate

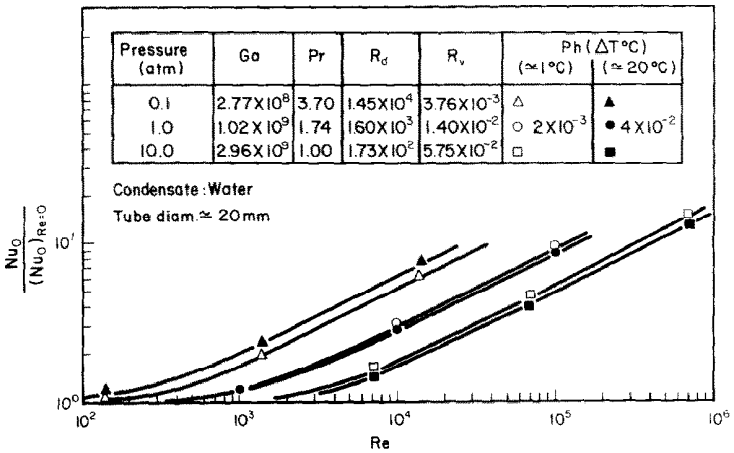

FIG. 7. Ratio $[(Nu_0)_{Re\neq 0}/(Nu_0)_{Re=0}]$ for water at different pressures as a function of the Reynolds number.

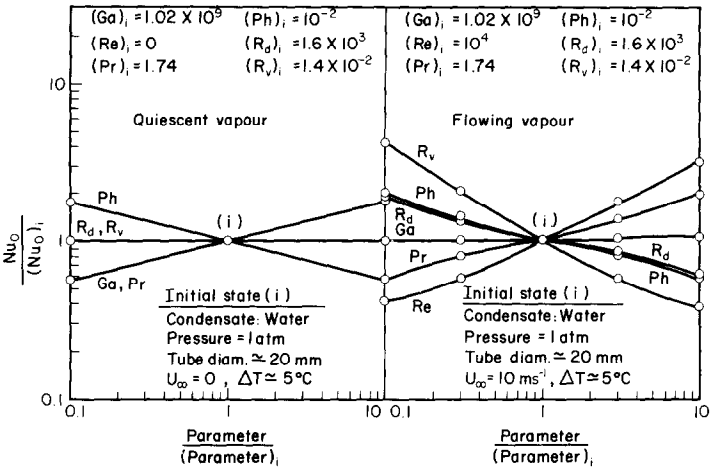

FIG. 8. The functional dependence of the local Nusselt number Nu_0 on the governing parameters for water near atmospheric conditions.

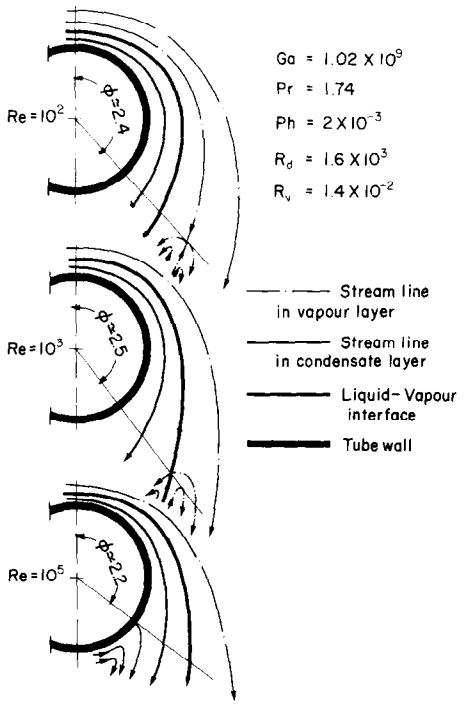

FIG. 9. Flow separation for water at 1 atm and different values of the Reynolds number.

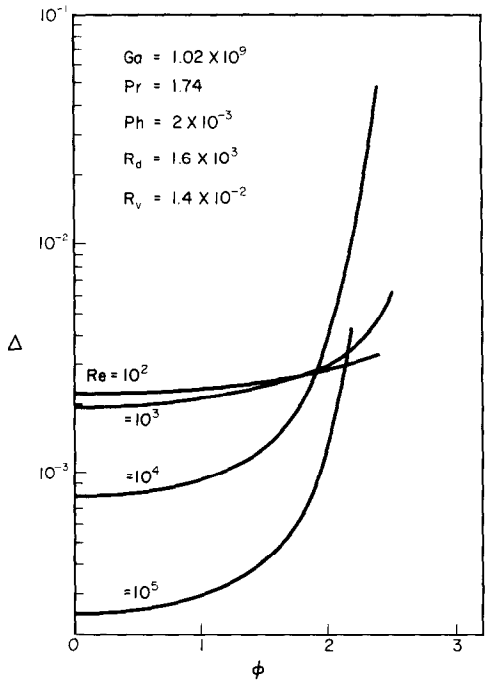

FIG. 10. Condensate layer thickness for water at 1 atm and different values of the Reynolds number.

layer does not occur in the vicinity of the solid wall. Examining the motion of the liquid-vapour interface shows that $(\partial u_l/\partial y)_{y=0} = 0$ at $\phi \simeq 2.0$ $[(u_l)_{y=0} \neq 0]$. At $\phi \simeq 2.5$ the liquid-vapour interface velocity is zero; the vapour in the vicinity of the interface moves opposite to the liquid. At $\phi > 2.5$, reversed motion exists partly in the condensate—and partly in the vapour layer. The condensate layer near the solid surface still moves in the main flow direction. At $Re = 10^5$ neither u_l nor $\partial u_l/\partial y$ vanishes at the liquid–vapour interface. However, $\partial u_l/\partial y = 0$ at the solid surface at $\phi \simeq 2.2$. The region of reversed motion is contained entirely in the condensate layer. A sketch of the stream lines in the three discussed cases is shown in Fig. 9 and the local thickness of the dimensionless condensate layer at different Reynolds numbers is shown in Fig. 10.

REFERENCES

1. W. Nusselt, Die Oberflächenkondensation des Wasserdampfes, *Z. Ver. Dt. Ing.* **60**, 541–546; 569–575 (1916).
2. E. M. Sparrow and J. L. Gregg, Laminar condensation heat transfer on a horizontal cylinder, *J. Heat Transfer* **81C**, 291–296 (1959).
3. M. M. Chen, An analytical study of laminar film con-

densation: Part 2—Single and multiple horizontal tubes, *J. Heat Transfer* **83C**, 55–60 (1961).
4. I. G. Shekriladze and V. I. Gomelauri, Theoretical study of laminar film condensation of flowing vapour, *Int. J. Heat Mass Transfer* **9**, 581–591 (1966).
5. V. E. Denny and A. F. Mills, Laminar film condensation of a flowing vapour on a horizontal cylinder at normal gravity, *J. Heat Transfer* **91C**, 495–501 (1969).
6. T. Fujii, H. Uehara and C. Kurata, Laminar filmwise condensation of flowing vapour on a horizontal cylinder, *Int. J. Heat Mass Transfer* **15**, 235–246 (1972).
7. M. Schmal, Eine Näherungslösung für die Kondensation von laminar strömendem Dampf mit beliebigen Druckgradienten bei kleiner Mach-Zahl und konstanten Stoffwerten, *Int. J. Heat Mass Transfer* **15**, 1137–1157 (1972).
8. S. Goldstein, Modern developments in fluid dynamics, Vol. 1, p. 149. Oxford University Press, London (1952).

SOLUTION DES EQUATIONS DE LA COUCHE LIMITE DIPHASIQUE POUR LA CONDENSATION LAMINAIRE EN FILM DE LA VAPEUR EN ECOULEMENT PERPANDICULAIRE A UN CYLINDRE HORIZONTAL

Résumé—On présente une méthode pour résoudre les équations de la couche limite diphasique pour la condensation de vapeur sur un cylindre horizontal. Les trois équations aux dérivées partielles sont transformées en équations différentielles dont le nombre dépend de la précision souhaitée. Les solutions numériques donnent la distribution des valeurs locales du nombre de Nusselt sur la périphérie du cylindre en fonction des différents paramètres actifs.

DIE LÖSUNG DER ZWEIPHASEN-GRENZSCHICHTGLEICHUNGEN FÜR LAMINARE FILMKONDENSATION AN EINEM VON DAMPF QUERÜBERSTRÖMTEN HORIZONTALEN ZYLINDER

Zusammenfassung—Es wird eine Methode zur Lösung der Zweiphasen-Grenzschichtgleichungen für die Beschreibung der Kondensation strömenden Dampfes an einem horizontalen Zylinder vorgestellt. Die das Problem beschreibenden drei partiellen Differentialgleichungen werden in gewöhnliche Differentialgleichungen umgewandelt, deren Anzahl von den Genauigkeitsanforderungen an die Lösung abhängt. Die numerischen Lösungen geben die Verteilung der lokalen Werte der Nußeltzahl über dem Umfang des Zylinders in Abhängigkeit von den Einflußgrößen wieder.

РЕШЕНИЕ УРАВНЕНИЙ ДВУХФАЗНОГО ПОГРАНИЧНОГО СЛОЯ ПРИ ЛАМИНАРНОЙ ПЛЕНОЧНОЙ КОНДЕНСАЦИИ ПАРА, ОБТЕКАЮЩЕГО ГОРИЗОНТАЛЬНЫЙ ЦИЛИНДР ПЕРПЕНДИКУЛЯРНО ЕГО ОСИ

Аннотация — Предлагается метод решения уравнений двухфазного пограничного слоя при конденсации пара на горизонтальном цилиндре. Система трех основных дифференциальных уравнений в частных производных преобразуется в систему обыкновенных дифференциальных уравнений, число которых зависит от требуемой точности решения. В результате численного решения получено распределение локальных значений числа Нуссельта по окружности цилиндра в зависимости от основных параметров.